Node-Specific Heritability in the Mouse Connectome

Nian Wang[1], Robert J Anderson[1], David G Ashbrook[2], Vivek Gopalakrishnan[3], Youngser Park[4], Carey E Priebe [4,5], Yi Qi[1], Joshua T Vogelstein[3,4,6,7], Robert W Williams[2], G Allan Johnson[1,8, *]

[1] Duke Center for In Vivo Microscopy, Department of Radiology, Duke University, Durham, North Carolina 27710, USA

[2] Department of Genetics, Genomics and Informatics, University of Tennessee Health Science Center, Memphis, TN 38163, USA

[3] Department of Biomedical Engineering, Johns Hopkins University, Baltimore, MD 21287, USA

[4] Center for Imaging Science, Johns Hopkins University, Baltimore, MD 21287, USA

[5] Department of Applied Mathematics and Statistics, Johns Hopkins University, Baltimore, MD 21287, USA

[6] Institute for Computational Medicine, Johns Hopkins University, Baltimore, MD 21287, USA

[7] Kavli Neuroscience Discovery Institute, Johns Hopkins University, Baltimore, MD 21287, USA

[8] Department of Biomedical Engineering, Duke University, Durham, NC 27710, USA

*Correspondence: gjohnson@duke.edu

HIGHLIGHTS

- Microscopic MRI/DTI connectomes were generated in 4 strains of mice (n=8/strain).
- Heritability of volume, and diffusion metrics was measured for 166 regions.
- Low dimensional scaling allowed robust comparison of connectome nodes.
- Volume, FA, AD, RD and connectome nodes are heritable in over 50% of the regions.

SUMMARY

MRI provides an opportunity to link neuroanatomic phenotypes to genetic expression. Genome-wide associative studies in the ENIGMA consortium and the UK Biobank have demonstrated significant links between brain structure and specific genes. Similar studies in rodents are challenging because of the scale. We report whole brain diffusion connectomes of four strains of mice (C57BL/6J, DBA/2J, CAST/EiJ, and BTBR) at spatial resolution 20,000 times higher than the human connectome. We derived volumes and scalar diffusion metrics for 322 regions of the brain. Volume was the most heritable trait followed by FA, RD, and AD. These traits were heritable in > 60% of the regions when comparing all four strains. Many were also highly heritable when the BTBR was not included. Using a unique statistical approach to limit false discovery allowed us to identify a number of specific brain nodes in which connectivity was highly heritable.

KEYWORDS
MRI/DTI, mouse brain, MR microscopy, connectome

INTRODUCTION

Genetic approaches have been used for over 40 years to study sources of natural variation in brain structure within humans and many other species. These approaches have ranged from electron microscopy (EM) of single neurons and their arborizations [1] to global studies of whole brain systems [2] [3] [4] [5] [6] [7-9].

The advent of structural and functional MRI has opened up new ways to systematically probe the influence of genetic variation, developmental stage, environmental factors, neurological, psychiatric and neurodegenerative disease on brain structure and function [2, 4, 7, 10]. Exploration of the genetic modulation of brain connectomes is a relatively new extension driven largely by powerful diffusion tensor imaging (DTI) methods that now have much higher throughput [4, 6]. While numerous studies have explored the genetic modulation of cortical and cerebellar volumes using MRI, there is now greater interest in the structural and functional connections—the connectomes of brain, and relations to variation in connectomes to variation in behavior, aging, and disease (e.g., the Human Connectome Project http://www.humanconnectomeproject.org/, the ENIGMA Consortium (http://enigma.ini.usc.edu/, and the ADNI collaboration http://adni.loni.usc.edu/).

Application of these MR methods in the rodent allows one to examine dimensions not readily available in the clinical setting and with significantly higher spatial resolution, despite much smaller absolute brain volumes [11] [3] [12]. Perhaps the most compelling advantage of rodent models is the ability to systematically control genomes, impact diseases, test treatments, and to obtain tissues and cells at different stages. This tight experimental control and the fact that one can study identical genomes multiple times

allows one to ask questions that usually cannot be addressed well in a clinical setting. For example, it is practical to study thousands of isogenic cases to accumulate massive omics datasets for a "given brain"— as done by the Allen Brain Institute to study brain gene expression [13].

One goal of this study is to take advantage of the isogenicity of four different strains of mice—C57BL/6J (B6), DBA/2J (D2), CAST/EiJ (CAST) and BTBR T+ *Itpr3*^{tf}/J (BTBR) to systematically map regional volume, DTI metrics, and connectomes for over 166 brain regions and fiber tracts. We have resampled each strain at a reasonable within-strain replication rate of eight per genome—four males and four females, all young adults at about 3 months-of-age. By carrying out the same MRI workflows across these four markedly different strains we are able to estimate heritabilities for large number of structures, parameters, and connectivities. We are also able to map the neuroanatomical distribution of both means and variances of the variables we have measured, and to test how the patterns of heritability highlight otherwise undetectable systems-level features. For example, do components of particular CNS systems tend to have higher or lower heritabilities due to relaxed or purifying selection? Do regions of the brainstem responsible for core homeostatic mechanisms have lower variation and lower heritability than forebrain structures?

The majority of the human studies are genome-wide association studies (GWAS) that have modest statistical power but the ability to define critical loci with a high degree of precision [14] [4]. Mouse linkage studies can provide the higher power of a family linkage study, albeit with lower precision. The availability of very large families of isogenic mice—for example, the BXD family—provides a middle ground, with good power and sub-centimorgan precision [15]. To date, the extension of quantitative connectomics to rodent neurogenetics has been limited. A number of investigators have studied regional volume changes and diffusion scalar metrics, e.g., fractional anisotropy (FA), axial diffusivity (AD), radial diffusivity (RD) and mean diffusivity (MD) in specific knockouts [16, 17]. But connectomic studies have been limited by the technical difficulties of scaling from the human brain (1500 g) to the mouse (0.45 g) [18-20]. The simultaneous demands of reducing voxel volume by at least 3000, providing sufficient diffusion weighting, sampling an adequate number of gradient angles, maintaining signal to noise, all while maintaining a reasonable scan time (under 24 hours), have made routine mouse brain connectomics challenging. All of this must be viewed in light of recent papers that have highlighted the problems of false negative tracts in structural diffusion connectomics [21] [22]. A single 1.25 mm^3 voxel, as used in the human connectome project, can encompass on the order of 100,000 neurons and their processes [23]. Errors in tractography resulting from crossing and merging fibers can result in substantial false positive connections. Mapping connectomics from human to mouse is technically challenging.

We have addressed many of the technical questions through the development of magnetic resonance histology, i.e. scans of postmortem tissue using a collection of unique hardware and adaptation of specialized encoding methods [24] [25]. We have validated the methods against retroviral tracers and gauged some of the limitations [20,

24]. And we have streamlined the methods to allow the higher throughput required for quantitative genomics [12, 24].

This paper applies state-of-the-art MRI workflows to study heritabilities at three different levels: (1) volumetrically-defined brain structures, including well over 150 regions of interest—both nuclei, cortical regions, and fiber tracts, (2) Scalar DTI parameters, and (3) variation in DTI-defined connectomes. For this initial work, we have used four fully inbred strains of mice at the same age used by the Allen Brain Atlas and with eight replicates each:

1. C57BL/6J (B6)—often referred to as "the mouse"—the references strain for murine genomics and neuroscience. B6 is the maternal strain of the large BXD family of strains (n of 150 progeny strains [15]). B6 is a member of the Mus musculus domesticus subspecies, and has a mean brain weight of 479 ± 3.7 mg (n = 259, all brain data generated in our laboratory using relatively uniform methods, [26] and www.mbl.org/references/BrainWeightOfStrainofMice.xlsx, and GeneNetwork trait 49909).
2. DBA/2J (D2)—the oldest fully inbred strain—and like B6, also well sequenced [27]. D2 is the other parent of the BXD family and a Mus musculus domesticus with a mean brain weight of 403 ± 4.5 mg (n = 154).
3. CAST/EiJ (CAST)—a fully inbred derivative of a wild Southeast Asian subspecies of Mus musculus (M.m, castaneus). This strain breeds well with other strains, and although somewhat smaller has a mean brain weight of 395 ± 4.6 mg m (n = 23).
4. BTBR T+ *Itpr3*^{tf}/J (BTBR)—a common inbred strain with well-known behavioral and neuroanatomical abnormalities [28] [29], including a highly penetrant callosal defect. A Mus musculus domesticus with a brain weight of 487 ± 3.9 very close to that of B6 (n = 51)

The first two strains were chosen to test sensitivity to detect relatively subtle phenotypic differences among two neuroanatomically normal strains. The specific long range goal was to validate and extend work using the BXD family, for which a very deep neuroanatomical and behavioral phenomes has already been assembled [15]. In contrast, CAST/EiJ and BTBR were chosen to maximize genetic and neuroanatomical variability, respectively. The choice of any four isogenic strains limits generality of findings, and means that estimates still have a narrow range of applicability, but with this level of within-strain replication, we can address the following questions:

- What is the heritability of brain structure volumes across the whole strain set and across specific subsets — for example the parents of the BXD family?
- To what extent do differences in heritabilities map onto conventional neuroanatomical divisions or systems?
- To what extent are heritabilities sensitive to the inclusion of different subspecies (CAST/EiJ) or known mutations (BTBR)?
- What are the relative heritablities of regional volumes and the scalar metrics generated by DTI?
- What image-based phenotypes derived from the connectome are heritable?
- Can one resolve regional heritability differences based on connectivity?

RESULTS

Whole Brain Population Atlases Provide Anatomic Detail

Figure 1 shows dorsal slices from the color fractional anisotropy (clrFA) image of the average male (n = 4) from each strain. The FA is a normalized ratio of the eigen values from the diffusion tensor which ranges from 0 (isotropic) to 1(anisotropic) [30, 31]. The white matter is anisotropic and the intensity of the FA images is linearly related to the anisotropy. Color has been added by encoding the direction of the principal eigen vector from the diffusion tensor. In this presentation, red is left/right, green is anterior/posterior, and blue is dorsal/ventral. The comparison shows morphologic differences as well as quantitative differences in the white matter anisotropy. The corpus callosum is much thicker and the saturation higher for the B6 indicating higher anisotropy. The corpus is thinner and the intensity lower in the D2 and CAST. The midline connection of the corpus is totally absent in the BTBR. More quantitative differences can be derived as seen below.

For each specimen there are ten different scalar images derived from the diffusion processing pipeline (See Methods). Each image highlights different anatomy in a complimentary fashion (See Figure S1) which is exploited in mapping the labels required for generating the connectomes (See Methods).

Multiple Brain Biomarkers are Heritable

A number of GWAS studies have demonstrated high heritability for volumes in multiple regions of the brain [14] [5, 6, 10, 32] Figure 2a is a plot of the heritability of strain means (H^2rix□) [33, 34]of the sub volumes in our mouse brain atlas that have been rank ordered from highest to lowest heritability. The plot includes the 166 regions of interest (ROI) for one hemisphere (See Methods). The volume of each sub region has been normalized to the total brain volume. The circles show the broad sense heritability when including all 4 strains. The stars exclude the BTBR, i.e. include only the B6, D2, and CAST. The color bar in each graph is a log scale of the value for that graph which allows one to appreciate any strong correlations with the magnitude of the metric and the rank order. The volume of all of the 166 sub regions is highly heritable (H^2rix□>0.8). As expected, the heritability drops when the BTBR is excluded. But the heritability of the group of similar strains is still very high (>0.8) for ~130 of the 166 total regions. The same trends are evident to a lesser extent when the same graphs are generated for broad-sense heritability (H^2, See Figure S2). The high heritability of strain means indicates that these traits will be amenable to linkage studies in populations derived from these inbred strains.

Figure 2b shows the heritability of FA with and without the BTBR. Again, the regions of interest are rank ordered. Nearly 150 regions have heritability >0.8 when the BTBR are included. When the BTBR are excluded, there is still a surprisingly large number of regions (~100) with heritability >0.8. The effects are similar for RD (Figure 2c) and AD (Figure 2d), with higher heritability for more regions when the BTBR are included. RD is slightly more heritable than AD. Both are slightly less heritable than FA which is derived from the two. The heritability of both is not strongly dependent on their value, i.e. the

heritability is not necessarily higher for larger values. Similar trends are seen for broad sense heritability (Figure S2).

Table 1 lists the top 20 regions from the rank ordered list for each of the scalar metrics in Figure 2 when comparing heritability for all four strains. Cerebellar white matter FA and FA from multiple regions of the cortex are highly heritable. Several regions are highlighted in both volume and diffusion changes, e.g. cingulate cortex- volume and FA; fimbria-volume, RD, and AD; lateral lemniscus- volume, FA and AD. And multiple regions have correlated heritability in AD, RD, and FA.

Figure S3 summarizes these results more globally. Volume is heritable in all the major subdivisions (isocortex, pallium, subpallium, diencephalon, midbrain, hindbrain and white matter) whether or not the BTBR is included. FA is similarly highly heritable in all regions with and without the BTBR. Perhaps the most curious findings are in the isocortex. FA is highly heritable when the BTBR is included or left out even though the absolute value of the FA is relatively low. The heritability of MD and RD drop significantly when the BTBR are removed from the analysis, suggesting there are significant differences in the underlying cytoarchitecture of the isocortex in the BTBR.

Average Connectomes are Generated for Each Strain

Figure 3 shows the average full connectome for all four strains: a) B6; b) D2; c) CAST; d) BTBR. The connection strength is shown with a log10 color scale. Each graph includes four sub sections: upper left- connections within left hemisphere, upper right- connections from left hemisphere to right, lower left- right hemisphere to left, and lower right- connections within right hemisphere. Figure S4 shows the order of seeds (top to bottom: isocortex, pallium, sb-pallium, diencephalon, midbrain, hindbrain and white matter) and targets (left to right: isocortex, pallium, subpallium, diencephalon, midbrain, hind brain and white matter) for each quadrant [20]. Direct comparison of connectomes is complicated by the problems of false discovery [35]. But visual comparisons do reveal differences between the BTBR (Figure 3d) and the other strains. Reduction between the hemispheres is evident when one looks at the upper right and lower left section of each quadrant. There are some intriguing differences between the more normal strains and the BTBR. The upper right-hand part of each quadrant shows connectivity between the isocortex and midbrain, hindbrain and white matter. The edge strengths in all of these regions is considerably reduced in the BTBR (Figure 3d) which is consistent with the observations in Figure S3.

Isogenic Comparisons Support Generation of a Heritability Adjacency Matrix

A crucial element of this study is the use of isogenic animals. This is apparent in Figure 2 (H^2rix) and Figure S2 (H^2) in the Supplement where the H^2rix is considerably higher for all the readouts (volume, AD, RD, FA). It makes possible the construction of Figure 4 which shows the strain mean heritability of the edges. The nodes in this graph are the same as those in Figure 3 and S4. But the matrix values are now the strain mean heritability (H^2rix) of the corresponding edge in the connectome. In Figure 4a each vertex is the result of 32 measurements of connection strength for that edge across the

entire population, i.e. with the inclusion of the BTBR. The color scale is no longer logarithmic as in Figure 3 across a logarithmic dynamic range. It is linear. Figure 4b shows the identical graph for n=24, i.e. the same population as in Figure 4a, less the BTBR. Inclusion of the BTBR results in higher heritability in connections between the two hemispheres arising from the known loss of connectivity across the midline, also seen in Figure 1d.

Table S1 lists the top 20 most heritable edges from Figure 4a. There are three edges (highlighted) that rise to the top 20 in both comparisons, i.e. with and without the BTBR. Inspection shows that the corpus callosum, the prominent phenotype for the BTBR is one of the more important nodes, in comparison of both groups. This is consistent with the subjective impression one derives from Figure 1 where both the morphologic structure and the intensity of the FA are visually different across the strains.

Omnibus Embedding Improves the Confidence in Comparisons

Figure 4 suggests that collections of edges in several regions have strong heritability. And subjective comparisons of connectomes in Figure 3 suggest regions where there are differences. But statistical comparisons are challenging. First, false discovery is a confound because of the size of the array (332x332). Secondly, the heritability calculations are essentially test statistics, whose sensitivity and specificity are dependent on the degree to which the data satisfy certain assumptions. While those assumptions are often appropriate, for these data, exploratory analysis demonstrates that they are not. Nonparametric methods for quantifying heritability fail to rectify this situation. Figure S5 demonstrates that there are no edges on their own that pass the typical 0.05 level of significance once conservatively correcting for multiple comparisons. Nonetheless, it is clear from the previous figures (Figure 3 and 4) that there are significant differences between the strains. The problem is that existing methods for quantifying these differences are not adequate. We therefore devised a new method for statistically determining heritability of connectomes. Rather than treating each edge as an independent object, we first assess whether the connectome, as a whole, is heritable. Indeed, as demonstrated by Figure 5a and 5b, the connectomes of a given strain tend to be more similar to one another than they are to other strains. Using classical multidimensional scaling to embed each connectome into just two dimensions, it becomes apparent that the connectomes tend to form strain-specific groups. This connectome-wide group effect is preserved both when including and excluding the BTBR strain. Given these results, the natural next question is which brain regions confer the resulting heritability.

To answer this question, we leverage recent developments in the statistical analysis of populations of graphs on a shared vertex set, to find a joint low-dimensional representation of each node in each connectome, based on its connectivity profile, that is, its set of connections. Doing so enables us to use standard methods for subsequent inference. In particular, we posit a multivariate non-parametric k-sample test hypothesis: for each node, is its low-dimensional representation for a given strain sampled from the same distribution as the other strains. Figure 5c shows that about 280 nodes, out of the

322 possible nodes, are significantly different across all four strains, after a stringent correction for false positives. Figure 5d shows the same analysis for the three control groups where now there are roughly 150 nodes that are significantly different. Moreover, there are multiple pairs of nodes where both hemispheres were significantly different. The top twenty are listed in Table 2.

Figure 6 shows the tractograms for four of the nodes in which the p values are the most significant, i.e. Table 2. The corpus callosum is profoundly different in the BTBR and it is the most highly ranked node when comparing all four strains. The termination at the mid line is obvious in Figure 6b. The corpus callosum is also highly heritable when the BTBR is excluded. And this is consistent with the anatomical observations from Figure 1 in both the morphology and intensity in the color FA. The substantia nigra, internal capsule and fimbria are the next three most highly ranked nodes when comparing all four strains. The internal capsule and substantia nigra are also in the top 4 when comparing the three similar strains suggesting that these regions are highly heritable across many strains. Examination of the tractograms affirms the statistical findings. Tracts across the midline are substantially reduced for the BTBR in the substantia nigra and internal capsule and clearly less dense in the contralateral side for the fimbria than the other three strains.

DISCUSSION

This study applies state-of-the-art MRI workflows to study heritabilities at three different levels: (1) volumetrically-define brain structures, including well over 100 regions of interest—both nuclei, cortical regions, and fiber tracts, (2) DTI parameters, and (3) variation in DTI-defined connectomes. For this initial work we have used four fully and isogenic inbred strains of mice that differ greatly in genome sequence-—from 5 to 15 million variants distinguishing any pair of strains.

The most important findings are:

Microscopic MRI/DTI Provides Quantitative Phenotypes

Brain connectomes can vary over an enormous range of scale, over species, and technologies. The electron microscopy connectome of the drosophila acquired at nanometer resolution is constructed at voxels on the order of 10^{-15} mm^3 [36]. Clinical MRI acquires data with voxels on the order of 2 mm^3[23]. The mouse brain data in these studies were acquired with voxels < 10^{-5} mm^3. Tract tracing in an EM image relies on different physical phenomena than a retroviral tracer which in turn is a considerably different tracing mechanism than diffusion. Thomas et al [21] and Maier-Hein et al [22] have explored the specificity and sensitivity of the diffusion based (human) connectome and concluded that there can frequently be more false positive connections than true positive connections. One explanation is that merging or crossing fibers can lead to errors in tracking. This observation has driven us to push the spatial/angular resolution (in rodents) by nearly 5 orders of magnitude over that of clinical scans to limit the

consequences of volume averaging [20]. The data reported here are to the best of our knowledge, the highest (spatial/angular) resolution available of genetically linked diffusion connectivity metrics in the mouse brain yet reported. And the limits of sensitivity and specificity have been carefully catalogued relative to retroviral tracers [20, 24]. Several investigators have used in vivo MRI to investigate structural connectivity in genetically engineered mice. Practical problems of life support limit the resolution in these studies to ~100x100x500 um with ~30 angular samples [37] [38]. Scans of post mortem specimens permit longer, higher resolution studies. Zhang et al reported some of the first DTI images of the post mortem mouse brain in 2002 [31] and have more recently used the method to understand the role of Bcl-x in brain development [39]. Subsequent studies have extended spatial resolution and applied the method to unraveling morphologic changes in genetic models of neurologic disease [16, 40]. These studies relied on the scalar metrics (AD, RD, FA etc.) but did not include any connectome. Generating the connectome adds a significant complication as one must acquire a "sufficient" number of angular samples to allow resolution of crossing and merging fibers. And the term "sufficient" has been a source of controversy. Calamante et al have developed higher resolution tract density methods for connectomics in post mortem specimens at 100 um^3 with 30 angular samples [41]. To enable comparison across the range of applications (human, mouse, in vivo, post mortem), we proposed the resolution index (RI), the product of the spatial and angular resolution [12]. RI for the human connectome is 128 [23]. RI for Calamante's study is 30,000 [41]. The RI for this work is >500,000.

Volume, FA, AD, RD, and Connectomes are Highly Heritable

Virtually all the scalar metrics we measured are heritable at some level in some regions. Multiple investigators have demonstrated heritability of volumes in specific sub regions of the brain in both human and rodent studies [42] [14] [43] [5]. Other recent studies have detected significant global heritability of FA, AD and RD in human populations [8] [9]. And multiple studies have demonstrated heritability of specific regions of connectivity, in human [44] [45]. However, this is one of the first to bring together a robust study of heritability of all of these metrics (volume, FA, AD, RD, connection strength) in the mouse. We have demonstrated region specific heritability of volume, FA, AD, RD and connectivity.

We evaluated three strains (B6, D2, CAST) where neuroanatomical and connectome differences were expected to be comparatively modest after correcting for global differences in brain volume, and one strain (BTBR) with major disruptions of interhemispheric connections. Working with isogenic animals (n = 8/strain) has allowed us to measure the within-strain variability of all traits with good precision, but with the caveat the we have sampled only a small number of genomes. The experimental design allowed us to test the methods in detection of major differences (e.g. the BTBR) where the anatomy is so different that one must be concerned about artifacts from label registration and other experimental errors in the processing pipeline.

There is a remarkably robust collection of heritable phenotypes. Volume is highly heritable across the entire range of the structures included. In a previous study, we demonstrated that genotype accounted for ~ 60% of the variability of volume differences in 33 regions of the brain of a cohort of C57BL/6 mice and nine different strains from the BXD family [3]. The average coefficient of variation of volume for the 33 structures across 10 strains was 7.5 ± 3.5%. These new studies provide the same data for 166 ROIs (in both hemispheres) with substantially improved precision. As seen in Figure S6, the coefficient of variation within a strain for the majority of the regions is ~5%. The heritability is not strongly dependent on the absolute volume of the structure. And more than 150 structures are highly heritable (>0.8). Previous GWAS studies have demonstrated heritability of volume in subcortical regions by aggregating data from fifty studies [6, 32]. The VETSA study compared 1,237 twins focusing on heritability of cortical thickness [46]. The ENIGMA consortium expanded on the heritability of subcortical structures by comparing lateral symmetry using 15,847 MRI scans from 52 different data sets [47]. A more recent study of data from the UK Biobank measured heritability across morphometric, diffusion and functional data in 8,428 individuals [10].

Kochunov et al demonstrated that whole brain FA and RA had strong genetic dependence while the genetic link to AD was not significant [8]. A twin study by Gustavson et al revealed that all of the regions they measured were heritable and FA and MD accounted for roughly half the heritability in the tract subdivision [48]. Recent studies from the UK Biobank have explored a number of image derived phenotypes demonstrating regional heritability of FA, AD and RA [10]. Our work shows similar results with FA having the highest heritability of the scalar diffusion metrics. In the full group (including BTBR), the FA is strongly heritable (>0.8) in ~130 of 166 regions of interest. Surprisingly, in the smaller group of more similar strains heritability is still >0.8 in over 100 of the ROIs. AD and RD are not as strongly linked. But heritability is still >0.8 in 50 ROIs (for RA) and ~30 ROIs for AD.

Finally, the Human Connectome Project has generated multiple studies of heritability of specific structural circuits in the brain. Figure 5 in this work shows again, a remarkably rich set of vertices (~280) with strong heritability. As with the scalar metrics (Figure 2), the evidence of genetic dependence in the connection strength is still there when the BTBR strain is removed from the analysis. Statistically robust comparison of connectomes is challenging because of false discovery. Trends that seem apparent in the color-coded adjacency matrices are influenced by our brain's ability to integrate the patterns. Creation of a connectivity profile for each node exploits this effect yielding a more statistically method to define those nodes that have the most statistically robust difference across the strains.

The brain is the most complicated organ in the body. Understanding its genetic underpinnings starts with an understanding of the structure. But the structure is fractal with collections of neurons linked through axons, collections of axons linked to local circuits, circuits classified as short or long range. No single view or scale provides a complete picture and no single method is sufficient. Unwinding the genetic links to brain structure provides a crucial role to understanding so many diseases, autism, dementia

and Alzheimer's disease. Sorting through the extraordinary complexity of these data can quickly become overwhelming. Rank ordering the scalar metrics and the most critical nodes in the connectome helps bring specific circuits in focus. Sophisticated network analysis can then be used to construct hypotheses connecting structural changes to behavior. The methods shown here allow one to span the scale from meso to micro over the whole brain. When coupled to the power provided through isogenic colonies promises a statistically robust approach to linking connectome to genome.

STAR METHODS

Detailed methods are provided in the online version of this paper and include the following:

- LEAD CONTACT AND DATA AVAILABILITY
- EXPERIMENTAL MODEL AND SUBJECT DETAILS
- METHOD DETAILS
- Image Acquisition
- Image Registration
- Connectome Generation
- DATA AVAILABILITY

LEAD CONTACT AND DATA AVAILABILITY

Further information and requests for data should be directed to the Lead Contact, G. Allan Johnson, (gjohnson@duke.edu)

EXPERIMENTAL MODEL AND SUBJECT DETAILS

All studies were performed under protocols approved by the Duke Institutional Animal Care and Use Committee (IACUCC). We choose four strains for comparison.

1. C57BL/6J (B6)—often referred to as "the mouse"—the references strain for murine genomics and neuroscience. B6 is the maternal strain of the large BXD family of strains (*n* of 150 progeny strains; [15]). B6 is a member of the *Mus musculus domesticus* subspecies, and has a mean brain weight of 479 ± 3.7 mg (*n* = 259, all brain data generated in our laboratory using relatively uniform methods, [26] and www.mbl.org/references/BrainWeightOfStrainofMice.xlsx, and GeneNetwork trait 49909).
2. DBA/2J (D2)—the oldest fully inbred strain—and like B6, also sequenced [27]. D2 is the other parent of the BXD family, a *Mus musculus domesticus* with a mean brain weight of 403 ± 4.5 mg (n = 154).
3. CAST/EiJ (CAST)—a fully inbred derivative of a wild Southeast Asian subspecies of *Mus musculus (M. m, castaneus).* This strain breeds well with other strains, and although somewhat smaller has a mean brain weight of 395 ± 4.6 mg m (*n* = 23).

4. BTBR T+ *Itpr3*^{tf}/J (BTBR)—a common inbred strain with well-known behavioral and neuroanatomical abnormalities including a highly penetrant callosal defect [28] [29] [49]. A *Mus musculus domesticus* with a brain weight of 487 ± 3.9 mg very close to that of B6 (*n* = 51)

The first three were chosen to test the ability of our protocols to distinguish more subtle differences in the volumes, DTI parameters, and connectomes. All three have normal CNS structure but nearly a 20% range of difference in total mean brain weights and volumes with B6 and BTBR having larger brains and D2 and CAST/Ei having smaller brains [15]. In contrast, BTBR has substantially abnormal brain structure that impacts forebrain commissures [28] [29] [49]

Four males and four females for each strain were purchased from The Jackson Laboratory. Brains were actively stained using methods outlined in detail previously. The method fixes the tissue and infuses Prohance, a Gd contrast agent, that reduces the spin lattice relaxation time (T1) [11]. The mandible was removed to allow use of a smaller radiofrequency coil and the specimens mounted in a 12 mm diameter plastic cylinder. The cylinder was filled with fomblin, an inert fluorocarbon that reduces susceptibility artefacts. All cases were young adults at 90 days of age.

METHOD DETAILS

Image Acquisition

MR images were acquired on a 9.4T vertical bore magnet with Resonance Research gradients providing ~2000 mT/m maximum gradient. The system is controlled by an Agilent Direct Drive console. Specimens were mounted in a 12 mm diameter single sheet solenoid radiofrequency coil. Three-dimensional (3D) diffusion weighted images were acquired with a Stejskal Tanner rf refocused spin echo sequences with TR/TE of 100/12.7 ms and b values of 4000 s /mm^2. Forty-six volumes were acquired, each with a different gradient angle along with 5 baseline (b0) images distributed throughout the four-dimensional (4D) acquisition. Sampling angles were uniformly distributed on the unit sphere. Compressed sensing was used with an acceleration of 4 X to reduce the acquisition time to 23.2 hrs/specimen [24]. The result is a 4D image array with isotropic spatial resolution of 45 um (voxel volume of 91 pl).

Image Registration

The 4D array (256x256x420x51) was passed to a post processing pipeline that first registered the five b0 images together. Then each of the diffusion weighted 3D volumes was registered to this average to correct for eddy current distortion. The registered 4D array was passed to DSI Studio which generated scalar images (AD, RD, FA, ClrFA) using the DTI model and NQA- normalized quantitative anisotropy and color NQA images using generalized q sampling [50]. Representative images (Figure S1) demonstrate the complimentary anatomic detail provided by these scalars to assist in the label registration.

A 3D label set was registered onto each 4D volume in that volume's native reference frame i.e. the reference frame in which the data were acquired. Waxholm Space (WHS)

[51], an isotropic label set for the mouse brain was expanded by Calabrese et al was extended with an additional 18 regions of interest yielding 166 regions of interest on each half of the brain [20]. A symmetric label set was generated by reflecting the label set through the midline. The symmetrized label set helps minimize bias in lateral comparisons [52]. The complete list of labels is available in the Supplemental material (Table S2). The labels are isotopic, i.e. they extend in all three planes at the same spatial resolution (45um) (Figure S7).

Figure S8 summarizes the path of the labels from the WHS atlas to the individual specimen [53]. Left and right labels were generated for each of the 32 specimens by creating a strain- and subject-specific spatial mapping to WHS. These are the source images (DWI, FA, AD, RD) referred to here as "WHS-Atlas", including the label set of 166 regions per side. Since there were significant anatomic differences between the strains which might push the registration pipeline beyond its capabilities, an intermediate hybrid average was generated for each strain. Averages were generated using a pipeline incorporating ANTS [54] with the following steps: (1) an automated skull stripping algorithm removed all the external tissue from the DWI and FA images; (2) A second stage of affine transform was applied, again using the DWI; (3) Six iterations of non-linear registration were performed using the diffeomorphic Symmetrized-Normalization algorithm as implemented in the Advanced Normalization Tools software [54, 55], and was driven by the FA contrast. After each diffeomorphic warp, images were averaged to create a new template. An average of all the inverse warps was then applied incrementally to move the shape of this template towards the median shape of the group before being used as the target of the next iteration. The strain averages were created from 8 specimens in that strain. Hybrid averages were created by averaging the 8 B6 with the 8 data volumes of the strain to which the labels were being mapped. Linear registrations used the Mattes similarity metric, while non-linear jobs used cross-correlation. The pipeline and validation have been described fully in [53]. For D2, the WHS-symmetric labels were warped using the appropriate transform chain and nearest neighbor interpolation such that each template had its own unedited label set. Before being propagated to the individual specimens, the template labels in the strain average were inspected and manually edited. It was necessary to refine the white matter of the cerebellum via thresholding of the template FA image. D2 and CAST required slight manual edits, primarily involving the boundary of the Caudate Putamen, while significant edits were made to the BTBR template labels due to notable anatomical differences in the cortex and midline structures. To minimize any artificial left-right asymmetric biases that might have been manually introduced during label editing, a symmetrized version of each strain template was created by mirroring the left or right side of the images and labels to the opposite side. For each subject, one last FA-driven non-linear registration was performed between it and its symmetrized template, and the left-derived and right-derived labels were accordingly mapped to the data as it was acquired. The decision to use the left- or right-derived data was made by measuring the coefficient of variation (CoV) of the left and right volumes for each structure for all specimens, and observing which side featured the lowest average CoV. Mapping a given specimen into the appropriate atlas allowed one to apply the symmetric labels and then transform the data back to native space.

Connectome Generation

Tracts were generated using the generalized Q-sampling (GQI) fiber tracking algorithm in DSI studio with a maximum of 3 fibers per pixel [56]. The propagation direction was calculated by applying trilinear interpolation on the fiber orientations provided from neighborhood voxels. The next point was then determined by moving in the propagation direction 0.02 mm. The propagation process was repeated until the tracking trajectory exceeded either a turning angle of greater than 45°, or the anisotropy value of the current position was below a predetermined threshold. Two million fibers were generated with whole brain seeding. For whole brain tractography (white matter and gray matter), the FA threshold was 0.1 with a minimum fiber length of 0.5 mm. Five million fibers were generated with whole brain seeding.

Whole brain connectomes were generated for each specimen in DSI studio using the registered label set with 166 regions of interest on each hemisphere. The seed and target regions were ordered based on their developmental origins. A complete key for region number and its anatomical definition is included in the supplemental information.

DATA AVAILABILITY

Scalar data for each specimen were aggregated into a single Excel sheet which contained two separate lists (left and right hemisphere) for all 166 labels followed by volume, mean value of FA, AD, RD for each sub region. Volume data for each sub region of a given strain were normalized to the total brain volume of that strain. The data package for each specimen consists of 51 unregistered 3D MRI volumes; a registered 4D volume; scalar images; mean values from the 166 regions for the scalars; tractography files from DSI studio; and connectomes. The aggregated data set is > 500 GB. Representative data are available from our website (https://civmvoxport.vm.duke.edu/voxbase/studyhome.php?studyid=402). User access is acquired with the
username: heritability
password: connectome

Access for additional data is provided through request at the same url.

ACKNOWLEDGEMENTS

This work was supported by NIH Grant 1 R01NS096720 (NW, GAJ), the XDATA program of the Defense Advanced Research Projects Agency (DARPA) administered through Air Force Research Laboratory contract FA8750-12-2-0303 (JTV, CEP, YP, VG), NSF 16-569 NeuroNex Award Number EEC-1449501 (JTV), NIGMS R01GM123489 (DA, RW) and NIA R01AG043930 (DA, RW). We are grateful to Gary Cofer, James Cook, and Lucy Upchurch for invaluable technical assistance. We thank Tatiana Johnson for special care in manuscript preparation and submission.

AUTHOR CONTRIBUTION

NW acquired the DTI data, performed much of the data reduction, generated most of the figures and assisted in writing the manuscript. RJA developed the annotation set, performed the label registrations and assisted in preparing figures. DGA assisted in the heritability analysis, generation of figures and writing the manuscript. VG, YP, CEP, and JTV developed the statistical approaches, assisted in preparation of figures. JYV assisted in manuscript preparation. YQ performed tissue preparation and managed data provenance. RWW and GAJ designed the experiment and wrote the manuscript.

DECLARATION OF INTERESTS

The authors declare no competing interests.

FIGURE LEGENDS

Figure 1: Population atlas (n=4) for the males in each strain. Dorsal color FA images from a) C57BL/6J; b) DBA/2J; c) CAST/EiJ; d) BTBR T+ *Itpr3*^{tf}/J. The corpus callosum (arrow) and fimbria are considerably thicker in the C57BL/6J than in the DBA/2J and CAST/EiJ. The corpus callosum is missing across the midline in the BTBR T+ *Itpr3*^{tf}/J.

Figure 2: Multiple Biomarkers are Heritable. Heritability of strain means (H^2rix□) heritability vs rank ordered ROI for a) ROI volume; b) mean ROI fractional anisotropy; c) mean ROI radial diffusivity; d) mean ROI axial diffusivity. Circles show H^2rix□ when all four strains are considered. Stars show H^2rix□ when the BTBR is excluded. The color scale in each plot is a log for the value of that index (volume, fa, radial diffusivity, or axial diffusivity).

Figure 3: Average connectome for each strain. Average connectomes (n=8) of a) C57; b) DBA2, and c) CAST strains are similar. The average connectome of d) the BTBR is significantly different with the reduced connectivity evident from the increased number of holes (dark blue entries). The seed nodes (rows) and targets (columns) are ordered according to the developmental origins.

Figure 4: Heritability Adjacency Matrix. Heritability of strain means (H^2rix□) of the edges (connection strengths) for a) all 4 strains (n=32) and b) excluding the BTBR (n=24).

Figure 5: Omnibus Embedding Improves the Confidence in Comparisons. Omnibus embedding facilitates statistical comparison using classical multidimensional scaling. A. The scatter plot shows clustering when the BTBR is included. B. When the BTBR is excluded, the clustering also shows statistical difference in the three similar

strains. C and D Plot of log (p-value) from manova comparisons in vertices across strain vs rank ordered vertex; C with BTBR and D without BTBR

Figure 6: Tractograms for the top 4 nodes. derived from the omni manova analysis including all four strain. A. B6, B. BTBR C. CAST D D2. The Corpus callosum, Substantia Nigra and internal capsule are also statistically different when the BTBR is excluded.

TABLES

Rank	Volume		AD		RD		FA	
1	5	A29a__Cingulate_Cortex	137	n8__Vestibulocochlear_Nerve	147	cbw__Cerebellar_White_Matter	147	cbw__Cerebellar_White_Matter
2	109	CoN__Cochlear_Nucleus	141	sc__Spinocerebellar_Tract	124	cg__Cingulum	27	S1FL__Primary_Somatosensory_Cortex
3	149	A25__Cingulate_Cortex	135	sp5__Spinal_Trigeminal_Nerve	118	ac__Anterior_Commisure	143	vsc__Ventral_Spinocerebellar_Tract
4	2	A24aPrime__Cingulate_Cortex	159	PaR__Pararubral_Nucleus	132	bsc__Brachium_of_Superior_Colliculus	19	M1__Primary_Motor_Cortex
5	143	vsc__Ventral_Spinocerebellar_Tract	126	vhc__Ventral_Hippocampal_Commissure	121	cc__Corpus_Callosum	132	bsc__Brachium_of_Superior_Colliculus
6	126	vhc__Ventral_Hippocampal_Commissure	96	Vll__Ventral_Lateral_Lemniscus_Nucleus	128	fr__Fasciculus_Retroflexus	146	icp_oc_tz__Inferior_Cerebellar_Peduncle
7	96	Vll__Ventral_Lateral_Lemniscus_Nucleus	120	fi__Fimbria	122	fx__Fornix	26	S1DZ__Primary_Somatosensory_Cortex
8	137	n8__Vestibulocochlear_Nerve	139	lfp__Longitudinal_Fasciculus_of_Pons	120	fi__Fimbria	28	S1HL__Primary_Somatosensory_Cortex
9	147	cbw__Cerebellar_White_Matter	13	DLO__Dorsolateral_Orbital_Cortex	146	cp_oc_tz__Inferior_Cerebellar_Peduncle	124	cg__Cingulum
10	63	GP__Globus_Pallidus	118	ac__Anterior_Commisure	84	RPC__Red_Nucleus_Parvicellular	153	MiTg__Microcellular_Tegmental_Nucleus
11	118	ac__Anterior_Commisure	60	Preoptic_Telencephalon	109	CoN__Cochlear_Nucleus	96	Vll__Ventral_Lateral_Lemniscus_Nucleus
12	92	Den__Dentate_(Lateral)_Nucleus_of_Cerebellum	146	icp_oc_tz__Inferior_Cerebellar_Peduncle	164	Prerubral_Forel	134	ll__Lateral_Lemniscus
13	123	st__Stria_Terminalis	17	LO__Lateral_Orbital_Cortex	131	pc__Posterior_Commissure	137	n8__Vestibulocochlear_Nerve
14	78	RTN__Reticular_Nucleus_of_Thalamus	109	CoN__Cochlear_Nucleus	108	Tg__Tegmental_Nucleus	80	DpMe__Deep_Mesencephalic_Nuclei
15	83	SN__Substantia_Nigra	150	das__Dorsal_Acustic_Stria	92	Den__Dentate_(Lateral)_Nucleus_of_Cerebellum	165	PVG_of_Hypothalamus
16	62	SPT__Septum	134	ll__Lateral_Lemniscus	95	FasMed__Fastigial_Medial_Nucleus_of_Cerebellum	41	VO__Ventral_Orbital_Cortex
17	1	A24a__Cingulate_Cortex	102	m5__Motor_Root_of_Trigeminal_Nerve	7	A29c__Cingulate_Cortex	13	DLO__Dorsolateral_Orbital_Cortex
18	105	Raphe_Nucleus	100	CG__Central_Gray	159	PaR__Pararubral_Nucleus	164	Prerubral_Forel
19	76	LGN__Lateral_Geniculate_Nucleus	131	pc__Posterior_Commissure	143	vsc__Ventral_Spinocerebellar_Tract	17	LO__Lateral_Orbital_Cortex
20	120	fi__Fimbria	41	VO__Ventral_Orbital_Cortex	106	Pr5__Trigeminal_Sensory_Nucleus	149	A25__Cingulate_Cortex

Table 1: Rank order of the heritability of volume and DTI metrics. A list of the top 20 heritable structures based on volume, AD, RD, and FA.

Rank	With BTBR		Without BTBR	
1	121	cc__Corpus_Callosum	127	ic__Internal_Capsule
2	249	SN__Substantia_Nigra	204	V2L__Secondary_Visual_Cortex
3	127	ic__Internal_Capsule	121	cc__Corpus_Callosum
4	286	fi__Fimbria	249	SN__Substantia_Nigra
5	299	cp__Cerebral_Peduncle	293	ic__Internal_Capsule
6	293	ic__Internal_Capsule	251	MRN__Midbrain_Reticular_Nucleus
7	66	Acb__Accumbens	252	RI__Rostral_Linear_Nucleus

8	287	cc__Corpus_Callosum	287	cc__Corpus_Callosum
9	62	SPT__Septum	77	ZI__Zona_Incerta
10	186	M2__Secondary_Motor_Cortex	83	SN__Substantia_Nigra
11	217	Hc__Hippocampus	133	cp__Cerebral_Peduncle
12	120	fi__Fimbria	66	Acb__Accumbens
13	178	AuV__Secondary_Auditory_Cortex	160	Retro_Rubral_Field
14	61	Sthal__Subthalamic_Nucleus Sthal	186	M2__Secondary_Motor_Cortex
15	65	Amy__Amygdala	132	bsc__Brachium_of_Superior_Colliculus
16	237	VTA__Ventral_Tegmental_Area	219	Ect__Ectorhinal_Cortex
17	133	cp__Cerebral_Peduncle	243	ZI__Zona_Incerta
18	292	vhc__Ventral_Hippocampal_Commissure	247	SC__Superior_Colliculus
19	289	st__Stria_Terminalis	202	V1B__Primary_Visual_Cortex
20	20	M2__Secondary_Motor_Cortex	229	GP__Globus_Pallidus

Table 2: List of the nodes with the lowest p values from the manova comparisons. The top 20 different nodes with BTBR and without BTBR. Left Hemisphere: ROI 1-166, Right Hemisphere: ROI 167-332. Color regions show the ROIs which appear in both comparisons (with and without BTBR).

REFERENCES

1. Goodman, C., *Isogenic Grasshoppers: Genetic Variability in the Morphology of Identified Neurons.* J Comp Neurol., 1978. **182**: p. 681-706.
2. Thompson, P.M., et al., *Genetic influences on brain structure.* Nature Neuroscience, 2001. **4**(12): p. 1253-1258.
3. Badea, A., G.A. Johnson, and R.W. Williams, *Genetic dissection of the mouse brain using high-field magnetic resonance microscopy.* Neuroimage, 2009. **45**(4): p. 1067-79.
4. Thompson, P.M., et al., *Genetics of the connectome.* NeuroImage, 2013. **80**: p. 475-488.
5. Ashbrook, D.G., et al., *Joint genetic analysis of hippocampal size in mouse and human identifies a novel gene linked to neurodegenerative disease.* BMC Genomics, 2014. **15**(1): p. 850-9.
6. Hibar, D.P., et al., *Common genetic variants influence human subcortical brain structures.* Nature, 2015. **520**(7546): p. 224-9.
7. Thompson, P.M., et al., *The ENIGMA Consortium: large-scale collaborative analyses of neuroimaging and genetic data.* Brain imaging and behavior, 2014. **8**(2): p. 153-182.
8. Kochunov, P., et al., *Heritability of fractional anisotropy in human white matter: A comparison of Human Connectome Project and ENIGMA-DTI data.* NeuroImage, 2015. **111**(C): p. 300-311.
9. Vuoksimaa, E., et al., *Heritability of white matter microstructure in late middle age: A twin study of tract-based fractional anisotropy and absolute diffusivity indices.* Hum Brain Mapp, 2017. **38**(4): p. 2026-2036.

10. Elliott, L.T., et al., *Genome-wide association studies of brain imaging phenotypes in UK Biobank.* Nature, 2018. **562**(7726): p. 1-17.
11. Johnson, G.A., et al., *High-throughput morphologic phenotyping of the mouse brain with magnetic resonance histology.* NeuroImage, 2007. **37**(1): p. 82-89.
12. Johnson, G.A., Wang, N, Anderson,R.J., Chen,M., Cofer,G.P., Gee, J.C., Pratson, F., Tustison,N., White, L.E. , *Whole mouse brain connectomics.* J Comp Neurol., 2018. **12**: p. 1-12.
13. Ng, L., et al., *An anatomic gene expression atlas of the adult mouse brain.* Nature Neuroscience, 2009. **12**(3): p. 356-362.
14. Stein, J.L., et al., *Identification of common variants associated with human hippocampal and intracranial volumes.* Nat Genet, 2012. **44**(5): p. 552-61.
15. Ashbrook, D.G., et al., *The expanded BXD family of mice: A cohort for experimental systems genetics and precision medicine.* bioRxiv, 2019. **1488**: p. 672097.
16. Bhagat, S.L., et al., *Mouse model of rare TOR1A variant found in sporadic focal dystonia impairs domains affected in DYT1 dystonia patients and animal models.* Neurobiology of Disease, 2016. **93**: p. 137-145.
17. Wang, X., et al., *Altered mGluR5-Homer scaffolds and corticostriatal connectivity in a <i>Shank3</i> complete knockout model of autism.* Nature Communications, 2016. **7**: p. 11459.
18. Daianu, M., et al., *Multi-Shell Hybrid Diffusion Imaging (HYDI) at 7 Tesla in TgF344-AD Transgenic Alzheimer Rats.* PLoS ONE, 2015. **10**(12).
19. Keifer, O.P., et al., *A comparative analysis of mouse and human medial geniculate nucleus connectivity: a DTI and anterograde tracing study.* NeuroImage, 2015. **105**: p. 53-66.
20. Calabrese, E., et al., *A diffusion MRI tractography connectome of the mouse brain and comparison with neuronal tracer data.* Cereb Cortex, 2015. **25**(11): p. 4628-4637.
21. Thomas, C., et al., *Anatomical accuracy of brain connections derived from diffusion MRI tractography is inherently limited.* Proceedings of the National Academy of Sciences of the United States of America, 2014. **111**(46): p. 16574-16579.
22. Maier-Hein, K.H., et al., *The challenge of mapping the human connectome based on diffusion tractography.* Nature Communications, 2017. **8**(1): p. 1349.
23. Ugurbil, K., et al., *Pushing spatial and temporal resolution for functional and diffusion MRI in the Human Connectome Project.* NeuroImage, 2013. **80**: p. 80-104.
24. Wang, N., et al., *Whole mouse brain structural connectomics using magnetic resonance histology.* Brain Structure and Function, 2018. **223**(9): p. 4323-4335.
25. Johnson, G.A., et al., *Whole mouse brain connectomics.* J Comp Neurol, 2018: p. 1-12.
26. Hager, R., et al., *Genetic architecture supports mosaic brain evolution and independent brain–body size regulation.* Nature Communications, 2012. **3**: p. 1079-5.
27. Wang, X., et al., *Joint mouse–human phenome-wide association to test gene function and disease risk.* Nature Communications, 2016. **7**: p. 1-13.
28. Ellegood, J., et al., *Neuroanatomical analysis of the BTBR mouse model of autism using magnetic resonance imaging and diffusion tensor imaging.* Neuroimage, 2013. **70**: p. 288-300.

29. Meyza, K.Z. and D.C. Blanchard, *The BTBR mouse model of idiopathic autism - Current view on mechanisms.* Neurosci Biobehav Rev, 2017. **76**(Pt A): p. 99-110.
30. Basser, P.J., J. Mattiello, and D. LeBihan, *MR diffusion tensor spectroscopy and imaging.* Biophys J, 1994. **66**(1): p. 259-67.
31. Zhang, J., P.C.M. van Zijl, and S. Mori, *Three-dimensional diffusion tensor magnetic resonance microimaging of adult mouse brain and hippocampus.* NeuroImage, 2002. **15**(4): p. 892-901.
32. Hibar, D.P., et al., *Novel genetic loci associated with hippocampal volume.* Nat Commun, 2017. **8**: p. 13624.
33. Belknap, J.K., *Effect of within-strain sample size on QTL detection and mapping using recombinant inbred mouse strains.* Behav Genet, 1998. **28**(1): p. 29-38.
34. Belknap, J.K., et al., *Type I and type II error rates for quantitative trait loci (QTL) mapping studies using recombinant inbred mouse strains.* Behav Genet, 1996. **26**(2): p. 149-60.
35. Zaletsky, A.C., L, Fornito,A,Murray, MM, Bullmore, E, *Connectivity differences in brain networks.* Neuroimage, 2012. **60**: p. 1055-1062.
36. Eichler, K., et al., *The complete connectome of a learning and memory centre in an insect brain.* Nature, 2017. **548**(7666): p. 175-182.
37. Arefin, T.M., et al., *Remodeling of Sensorimotor Brain Connectivity in Gpr88-Deficient Mice.* Brain connectivity, 2017. **7**(8): p. 526-540.
38. Hübner, N.S., et al., *The connectomics of brain demyelination: Functional and structural patterns in the cuprizone mouse model.* NeuroImage, 2017. **146**: p. 1-18.
39. Zhang, J., et al., *Magnetic resonance diffusion tensor microimaging reveals a role for Bcl-x in brain development and homeostasis.* Journal of Neuroscience, 2005. **25**(8): p. 1881-1888.
40. Jiang, Y. and G.A. Johnson, *Microscopic diffusion tensor imaging of the mouse brain.* NeuroImage, 2010. **50**(2): p. 465-471.
41. Calamante, F., et al., *Super-resolution track-density imaging studies of mouse brain: Comparison to histology.* NeuroImage, 2012. **59**(1): p. 286-296.
42. Peirce, J.L., et al., *Genetic architecture of the mouse hippocampus: identification of gene loci with selective regional effects.* Genes Brain Behav, 2003. **2**(4): p. 238-52.
43. Peper, J.S., et al., *Genetic influences on human brain structure: a review of brain imaging studies in twins.* Hum Brain Mapp, 2007. **28**(6): p. 464-73.
44. Zhang, Z., et al., *Mapping population-based structural connectomes.* NeuroImage, 2018. **172**: p. 130-145.
45. Yeh, F.-C., et al., *Population-averaged atlas of the macroscale human structural connectome and its network topology.* NeuroImage, 2018. **178**: p. 57-68.
46. Kremen, W., Prom_Wormley,E, et al *Genetic and Environmental Influences on the Size of Specific Brain Regions in Midlife: The VETSA MRI Study.* Neuroimage, 2010. **49**(2): p. 1213-1223.
47. Guadalupe, T., et al., *Human subcortical brain asymmetries in 15,847 people worldwide reveal effects of age and sex.* Brain imaging and behavior, 2017. **11**(5): p. 1497-1514.
48. *Predominantly global genetic influences on individual white matter tract microstructure.* NeuroImage, 2019. **184**: p. 871-880.

49. Faraji, J., et al., *Non-diagnostic symptoms in a mouse model of autism in relation to neuroanatomy: the BTBR strain reinvestigated.* Translational psychiatry, 2018. **8**(1): p. 234.
50. Yeh, F.-C., V.J. Wedeen, and W.-Y.I. Tseng, *Generalized q-Sampling Imaging.* IEEE Transactions on Medical Imaging. **29**(9): p. 1626-1635.
51. Johnson, G.A., et al., *Waxholm Space: An image-based reference for coordinating mouse brain research.* Neuroimage, 2010. **53**(2): p. 365-372.
52. Bowden, D.M., et al., *A symmetrical Waxholm canonical mouse brain for NeuroMaps.* Journal of Neuroscience Methods, 2011. **195**(2): p. 170-175.
53. Anderson, R.J., et al., *Small Animal Multivariate Brain Analysis (SAMBA) – a High Throughput Pipeline with a Validation Framework.* Neuroinformatics, 2018: p. 1-22.
54. Avants, B.B., Tustison, N.J., Wu, J., Cook, P.A., Gee, J.C., , *An open source multivariate framework for n-tissue segmentation with evaluation on public data. .* Neuroinformatics, 2011. **9**: p. 381-400.
55. Avants, B.B., Yushkevich, P., Pluta, J., Minkoff, D., Korczykowski, M., Detre, J., Gee, J.C., , *The optimal template effect in hippocampus studies of diseased populations.* Neuroimage, 2010. **49**: p. 2457-2466.
56. Yeh, F.-C., et al., *Deterministic Diffusion Fiber Tracking Improved by Quantitative Anisotropy.* PLoS ONE, 2013. **8**(11): p. e80713.

Table 1: Rank order of the heritability of volume and DTI metrics. A list of the top 20 heritable structures based on volume, AD, RD, and FA.

Rank	Volume		AD		RD		FA	
1	5	A29a__Cingulate_Cortex	13	n8__Vestibulocochlear_Nerve	14	cbw__Cerebellar_White_Matter	14	cbw__Cerebellar_White_Matter
2	10	CoN__Cochlear_Nucleus	14	sc__Spinocerebellar_Tract	12	cg__Cingulum	27	S1FL__Primary_Somatosensory_Cortex
3	14	A25__Cingulate_Cortex	13	sp5__Spinal_Trigeminal_Nerve	11	ac__Anterior_Commisure	14	vsc__Ventral_Spinocerebellar_Tract
4	2	A24aPrime__Cingulate_Cortex	15	PaR__Pararubral_Nucleus	13	bsc__Brachium_of_Superior_Colliculus	19	M1__Primary_Motor_Cortex
5	14	vsc__Ventral_Spinocerebellar_Tract	12	vhc__Ventral_Hippocampal_Commissure	12	cc__Corpus_Callosum	13	bsc__Brachium_of_Superior_Colliculus
6	12	vhc__Ventral_Hippocampal_Commissure	96	Vll__Ventral_Lateral_Lemniscus_Nucleus	12	fr__Fasciculus_Retroflexus	14	icp_oc_tz__Inferior_Cerebellar_Peduncle
7	96	Vll__Ventral_Lateral_Lemniscus_Nucleus	12	fi__Fimbria	12	fx__Fornix	26	S1DZ__Primary_Somatosensory_Cortex
8	137	n8__Vestibulocochlear_Nerve	139	lfp__Longitudinal_Fasciculus_of_Pons	120	fi__Fimbria	28	S1HL__Primary_Somatosensory_Cortex
9	147	cbw__Cerebellar_White_Matter	13	DLO__Dorsolateral_Orbital_Cortex	146	cp_oc_tz__Inferior_Cerebellar_Peduncle	124	cg__Cingulum
10	63	GP__Globus_Pallidus	118	ac__Anterior_Commisure	84	RPC__Red_Nucleus_Parvicellular	153	MiTg__Microcellular_Tegmental_Nucleus
11	118	ac__Anterior_Commisure	60	Preoptic_Telencephalon	109	CoN__Cochlear_Nucleus	96	Vll__Ventral_Lateral_Lemniscus_Nucleus
12	92	Den__Dentate_(Lateral)_Nucleus_of_Cerebellum	146	icp_oc_tz__Inferior_Cerebellar_Peduncle	164	Prerubral_Forel	134	ll__Lateral_Lemniscus
13	123	st__Stria_Terminalis	17	LO__Lateral_Orbital_Cortex	131	pc__Posterior_Commissure	137	n8__Vestibulocochlear_Nerve
14	78	RTN__Reticular_Nucleus_of_Thalamus	109	CoN__Cochlear_Nucleus	108	Tg__Tegmental_Nucleus	80	DpMe__Deep_Mesencephalic_Nuclei
15	83	SN__Substantia_Nigra	150	das__Dorsal_Acustic_Stria	92	Den__Dentate_(Lateral)_Nucleus_of_Cerebellum	165	PVG_of_Hypothalamus
16	62	SPT__Septum	134	ll__Lateral_Lemniscus	95	FasMed__Fastigial_Medial_Nucleus_of_Cerebellum	41	VO__Ventral_Orbital_Cortex
17	1	A24a__Cingulate_Cortex	102	m5__Motor_Root_of_Trigeminal_Nerve	7	A29c__Cingulate_Cortex	13	DLO__Dorsolateral_Orbital_Cortex
18	105	Raphe_Nucleus	100	CG__Central_Gray	159	PaR__Pararubral_Nucleus	164	Prerubral_Forel
19	76	LGN__Lateral_Geniculate_Nucleus	131	pc__Posterior_Commissure	143	vsc__Ventral_Spinocerebellar_Tract	17	LO__Lateral_Orbital_Cortex
20	120	fi__Fimbria	41	VO__Ventral_Orbital_Cortex	106	Pr5__Trigeminal_Sensory_Nucleus	149	A25__Cingulate_Cortex

Table 2: List of the nodes with the lowest p values from the manova comparisons. The top 20 different nodes with BTBR and without BTBR. Left Hemisphere: ROI 1-166, Right Hemisphere: ROI 167-332. Color regions show the ROIs which appear in both comparisons (with and without BTBR).

Rank	With BTBR		Without BTBR	
1	121	cc__Corpus_Callosum	127	ic__Internal_Capsule
2	249	SN__Substantia_Nigra	204	V2L__Secondary_Visual_Cortex
3	127	ic__Internal_Capsule	121	cc__Corpus_Callosum
4	286	fi__Fimbria	249	SN__Substantia_Nigra
5	299	cp__Cerebral_Peduncle	293	ic__Internal_Capsule
6	293	ic__Internal_Capsule	251	MRN__Midbrain_Reticular_Nucleus
7	66	Acb__Accumbens	252	RI__Rostral_Linear_Nucleus
8	287	cc__Corpus_Callosum	287	cc__Corpus_Callosum
9	62	SPT__Septum	77	ZI__Zona_Incerta
10	186	M2__Secondary_Motor_Cortex	83	SN__Substantia_Nigra
11	217	Hc__Hippocampus	133	cp__Cerebral_Peduncle
12	120	fi__Fimbria	66	Acb__Accumbens
13	178	AuV__Secondary_Auditory_Cortex	160	Retro_Rubral_Field
14	61	Sthal__Subthalamic_Nucleus Sthal	186	M2__Secondary_Motor_Cortex
15	65	Amy__Amygdala	132	bsc__Brachium_of_Superior_Colliculus
16	237	VTA__Ventral_Tegmental_Area	219	Ect__Ectorhinal_Cortex
17	133	cp__Cerebral_Peduncle	243	ZI__Zona_Incerta
18	292	vhc__Ventral_Hippocampal_Commissure	247	SC__Superior_Colliculus
19	289	st__Stria_Terminalis	202	V1B__Primary_Visual_Cortex
20	20	M2__Secondary_Motor_Cortex	229	GP__Globus_Pallidus

FIGURE 1

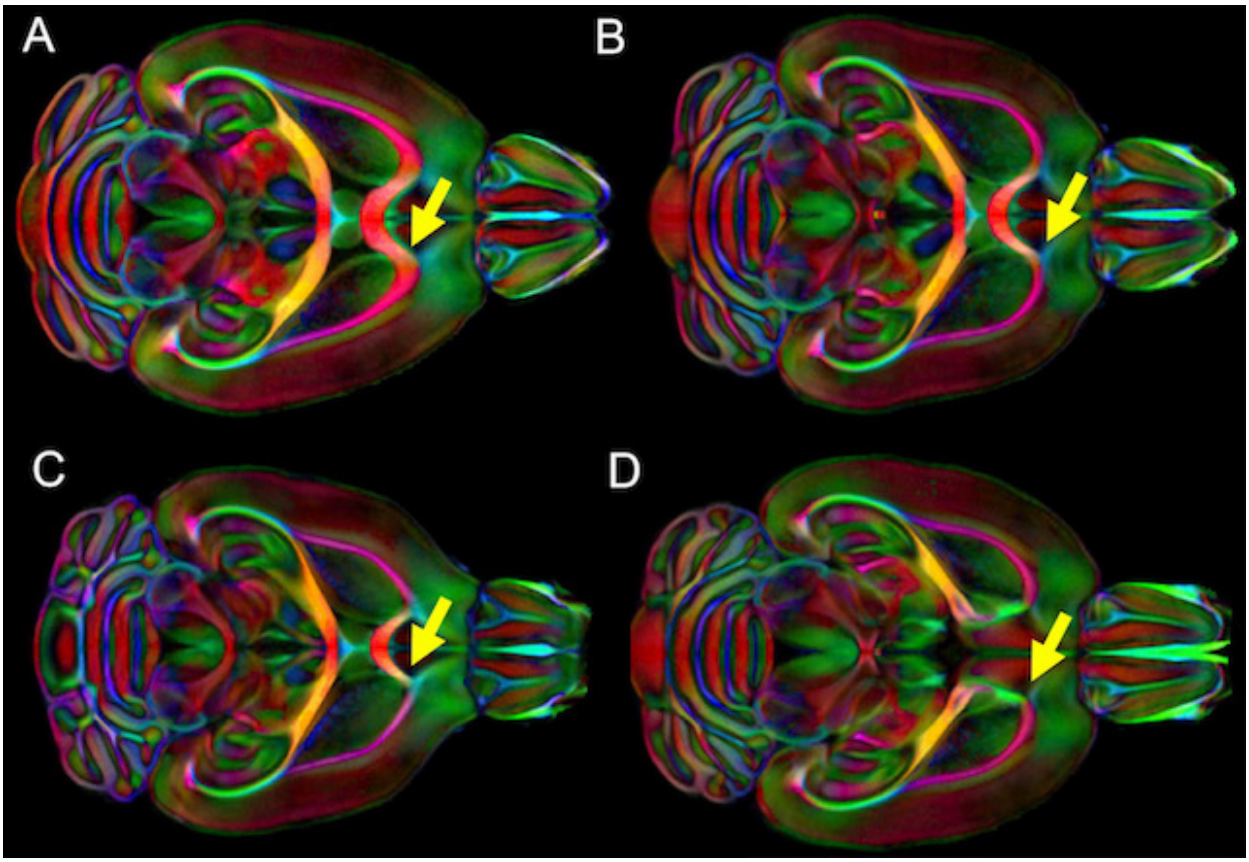

FIGURE 2

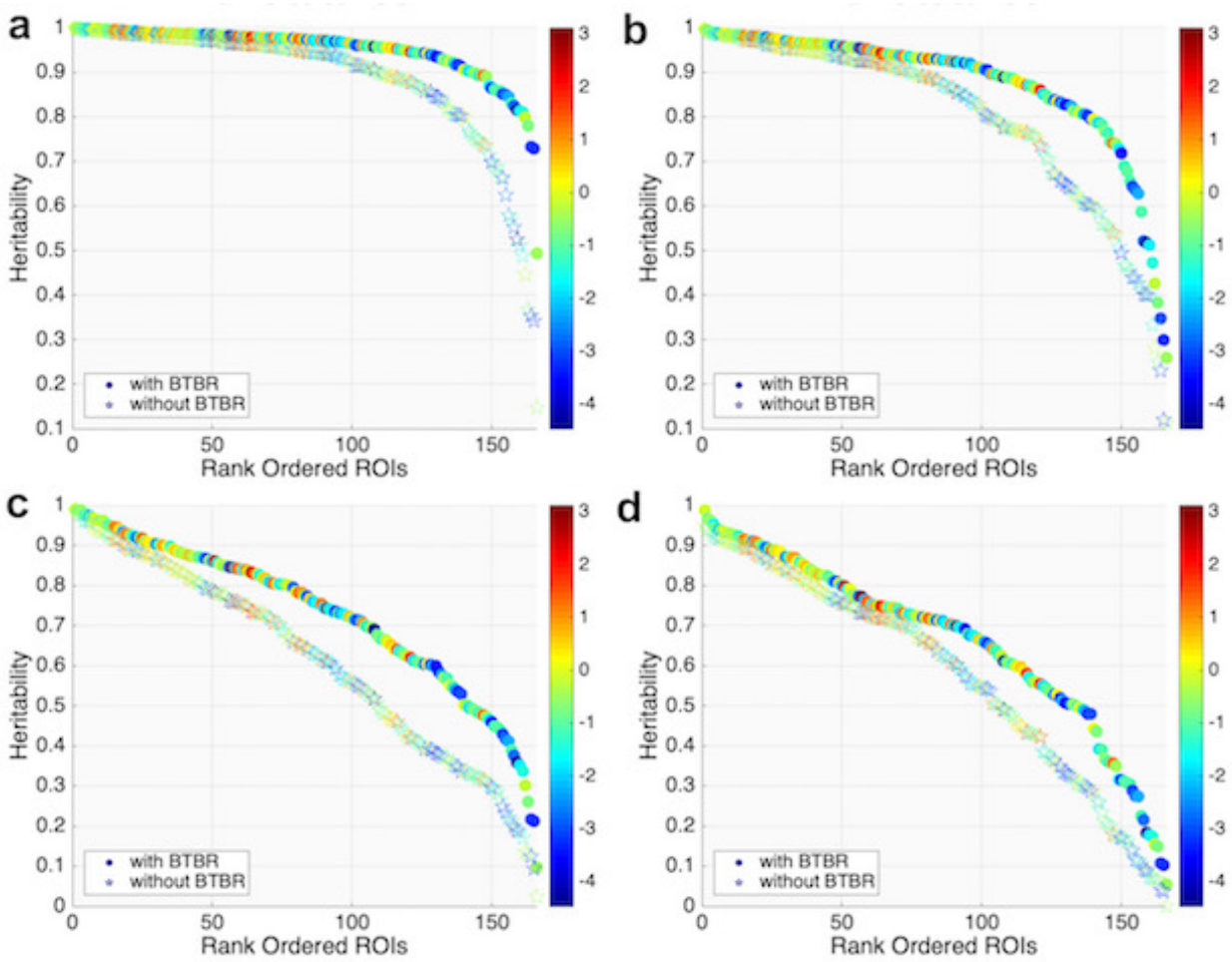
a
b
c
d
Heritability
Rank Ordered ROIs
with BTBR
without BTBR

FIGURE 3

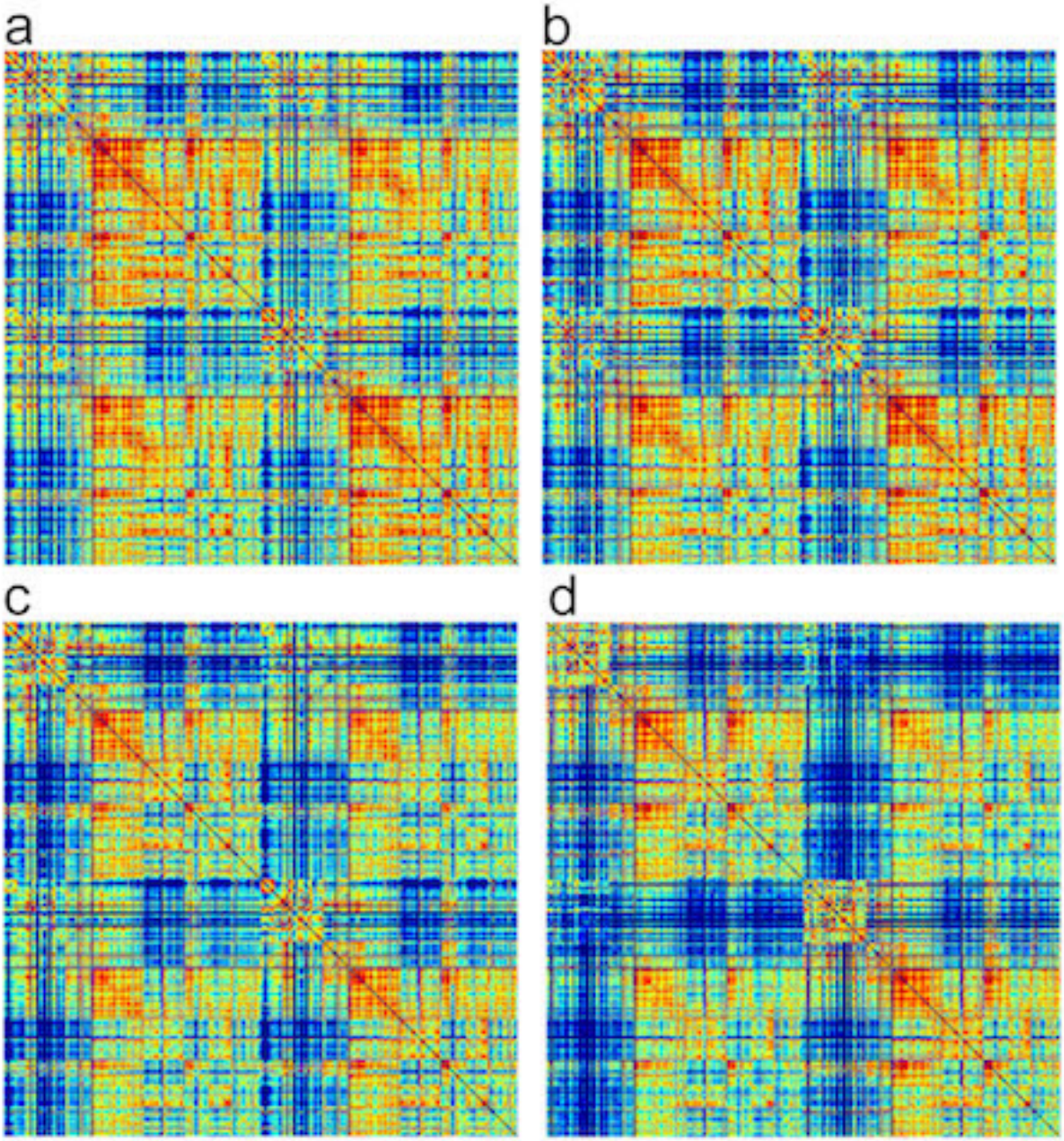

FIGURE 4

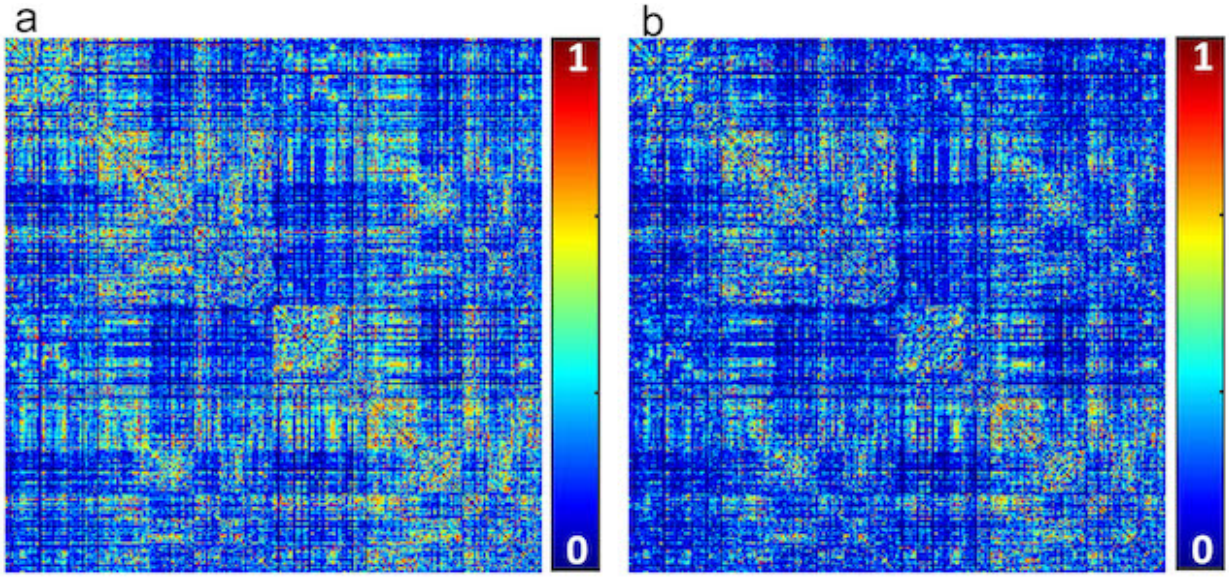

FIGURE 5

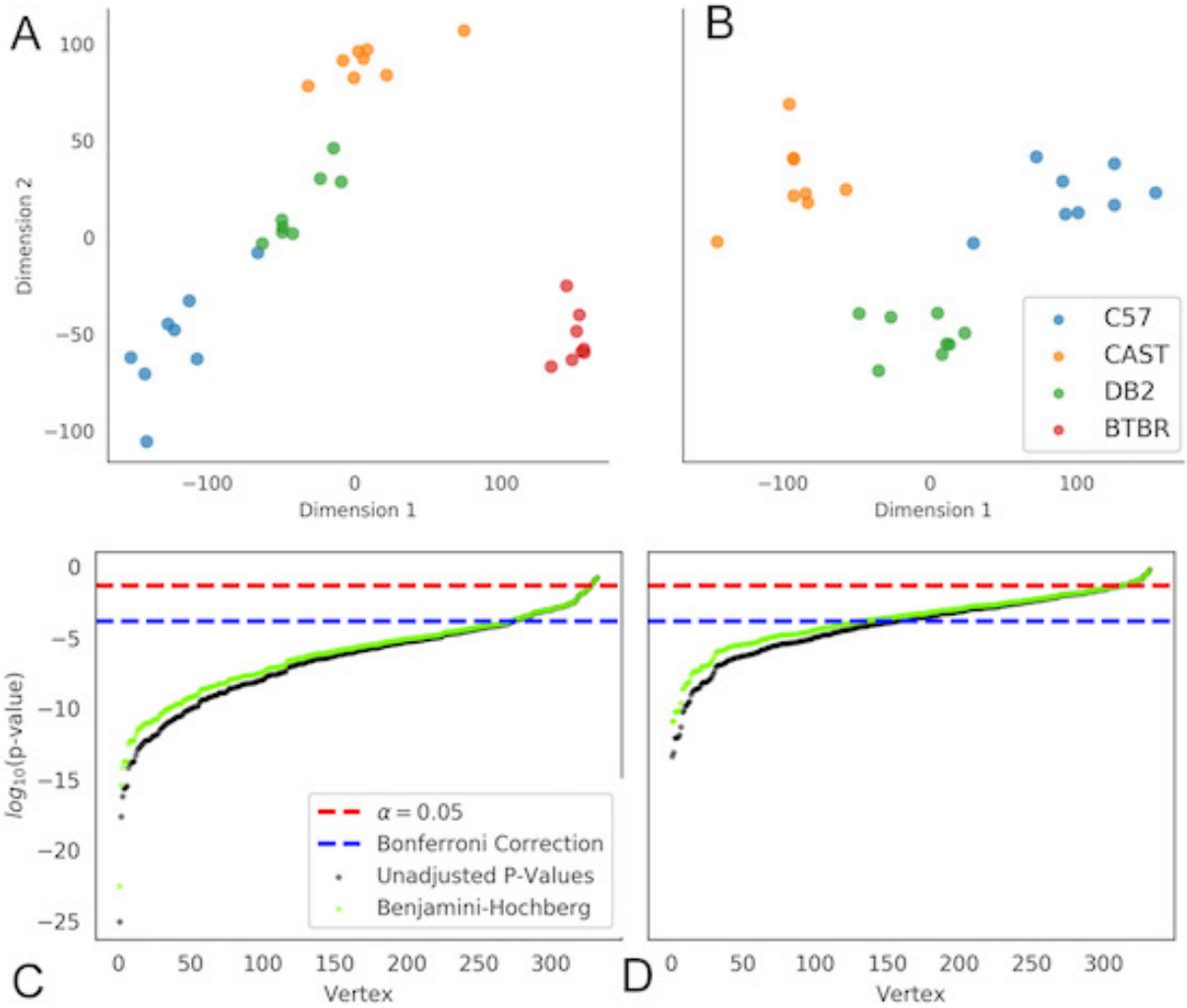
A
B
C
D
Dimension 1
Dimension 2
C57
CAST
DB2
BTBR
log_{10}(p-value)
Vertex
$\alpha = 0.05$
Bonferroni Correction
Unadjusted P-Values
Benjamini-Hochberg

FIGURE 6

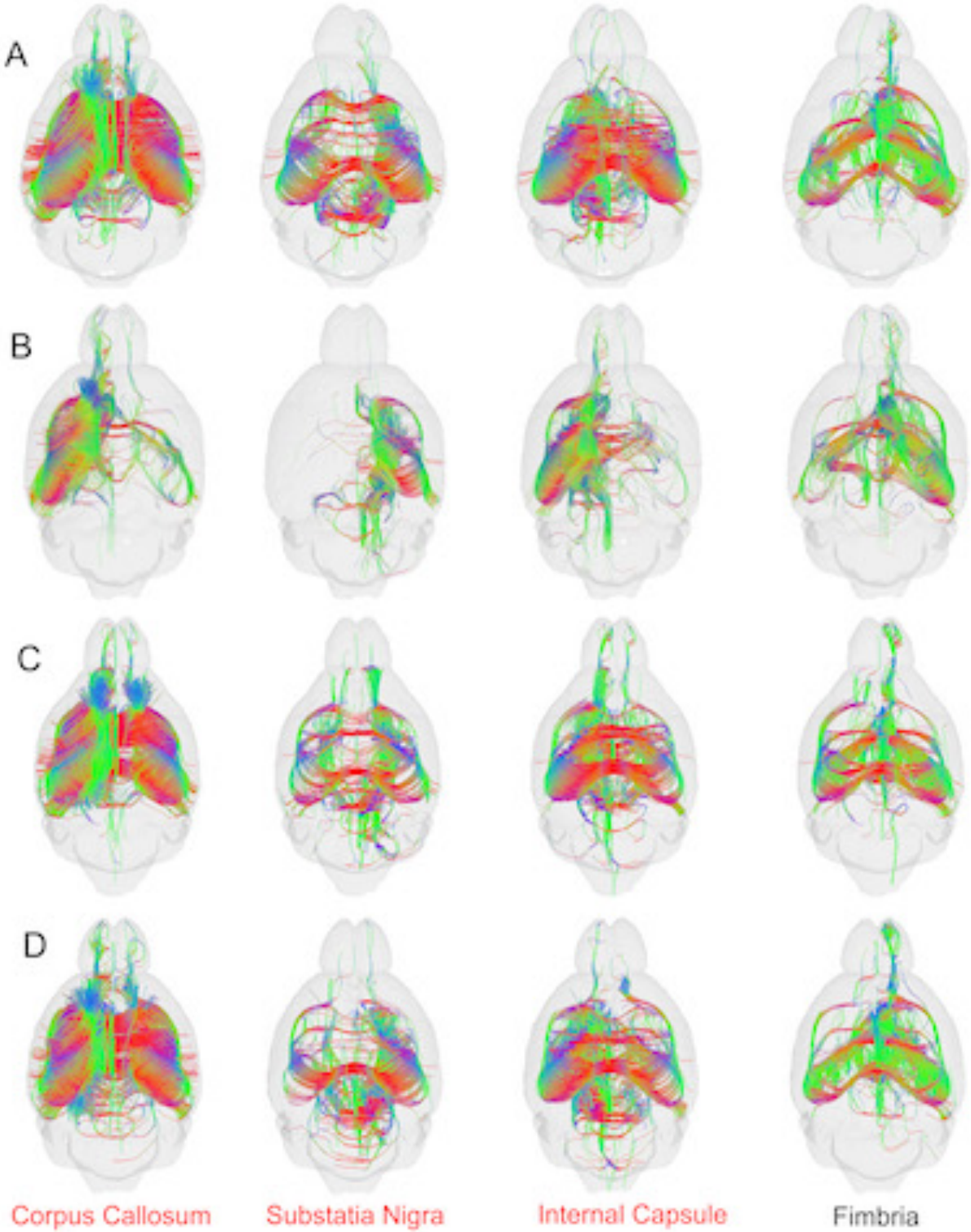
A
B
C
D
Corpus Callosum
Substatia Nigra
Internal Capsule
Fimbria